1

Introduction: A computational approach to multiphase flow

This book deals with multiphase flows, i.e. systems in which different fluid phases, or fluid and solid phases, are simultaneously present. The fluids may be different phases of the same substance, such as a liquid and its vapor, or different substances, such as a liquid and a permanent gas, or two liquids. In fluid–solid systems, the fluid may be a gas or a liquid, or gases, liquids, and solids may all coexist in the flow domain.

Without further specification, nearly all of fluid mechanics would be included in the previous paragraph. For example, a fluid flowing in a duct would be an instance of a fluid–solid system. The age-old problem of the fluid-dynamic force on a body (e.g. a leaf in the wind) would be another such instance, while the action of wind on ocean waves would be a situation involving a gas and a liquid.

In the sense in which the term is normally understood, however, *multiphase flow* denotes a subset of this very large class of problems. A precise definition is difficult to formulate as, often, whether a certain situation should be considered as a multiphase flow problem depends more on the point of view – or even the motivation – of the investigator than on its intrinsic nature. For example, wind waves would not fall under the purview of multiphase flow, even though some of the physical processes responsible for their behavior may be quite similar to those affecting gas–liquid stratified flows, e.g. in a pipe – a prime example of a multiphase system. The wall of a duct or a tree leaf may be considered as boundaries of the flow domain of interest, which would not qualify these as multiphase flow problems. However, the flow in a network of ducts, or wind blowing through a tree canopy, may be – and have been – studied as multiphase flow problems.

These examples point to a frequent feature of multiphase flow systems, namely the *complexity* arising from the mutual interaction of many subsystems. But – as a counterexample to the extent that it may be regarded as

'simple' – one may consider a single small bubble as an instance of multiphase flow, particularly if the study focuses on features that would be relevant to an assembly of such entities.

The interaction among many entities, such as bubbles, drops, or particles immersed in the fluid, is not the only source of the complexity usually exhibited by multiphase flow phenomena. There may be many other components as well, such as the very physics of the problem (e.g. the advancing of a solid–liquid–gas contact line, or the transition between different gas–liquid flow regimes), the simultaneous occurring of phenomena spanning widely different scales (e.g. oil recovery, where the flow at the single pore level impacts the behavior of the entire reservoir), the presence of a disturbed interface (e.g. surface waves on a falling film, or large, highly deformable drops or bubbles), turbulence, and others.

This complexity strongly limits the usefulness of purely analytical methods. For example, even for the flow around bodies with a simple shape such as spheres, most analytical results are limited to very small or very large Reynolds numbers. The more common and interesting situation of intermediate Reynolds numbers can hardly be studied by these means. When two or more bodies interact, or the ambient flow is not simple, the power of analytical methods is reduced further.

In a laboratory, it may even be difficult to set up a multiphase flow experiment with the necessary degree of control: the breakup of a drop in a turbulent flow or a precise characterization of the bubble or drop size distribution may be examples of such situations. Furthermore, many of the experimental techniques developed for single-phase flow encounter severe difficulties in their extension to multiphase systems. For example, even at volume fractions of a few percent, a bubbly flow may be nearly opaque to optical radiation so that visualization becomes problematic. The clustering of suspended particles in a turbulent flow depends on small-scale details which it may be very difficult to resolve. Little information about atomization can be gained by local probes, while adequate seeding for visualization may be impossible.

In this situation, numerical simulation becomes an essential tool for the investigation of multiphase flow. In a limited number of cases, computation can solve actual practical problems which lend themselves to direct numerical simulation (e.g. the flow in microfluidic devices), or for which sufficiently reliable mathematical models exist. But, more frequently, computation is the only available tool to investigate crucial physical aspects of the situation of interest, for example the role of gravity, or surface tension, which can be set to arbitrary values unattainable with physical experimentation.

Furthermore, the complexity of multiphase flows often requires reduced descriptions, for example by means of averaged equations, and the formulation of such reduced models can greatly benefit from the insight provided by computational results.

The last decade has seen the development of powerful computational capabilities which have marked a turning point in multiphase flow research. In the chapters that follow, we will give an overview of many of these developments on which future progress will undoubtedly be built.

1.1 Some typical multiphase flows

Having given up on the idea of providing a definition, we may illustrate the scope of multiphase flow phenomena by means of some typical examples. Here we encounter an embarrassment of riches. In technology, electric power generation, sprays (e.g. in internal combustion engines), pipelines, catalytic oil cracking, the aeration of water bodies, fluidized beds, and distillation columns are all legitimate examples. As a matter of fact, it is estimated that over half of anything which is produced in a modern industrial society depends to some extent on a multiphase flow process. In Nature, one may cite sandstorms, sediment transport, the "white water" produced by breaking waves, geysers, volcanic eruptions, acquifiers, clouds, and rain. The number of items in these lists can easily be made arbitrarily large, but it may be more useful to consider with a minimum of detail a few representative situations.

A typical example of a multiphase flow of major industrial interest is a *fluidized bed* (see Section 10.4). Conceptually, this device consists of a vertical vessel containing a bed of particles, which may range in size from tens of microns to centimeters. A fluid (a liquid or, more frequently, a gas) is pumped through the porous bottom of the vessel and through the bed. As the flow velocity is increased, initially one observes an increasing pressure drop across the bed. However, when the pressure drop reaches a value close to the weight of the bed per unit area, the particles become suspended in the fluid stream and the bed is said to be fluidized. These systems are useful as they promote an intimate contact between the particles and the fluid which facilitates, e.g., the combustion of material with a low caloric content (such as low-grade coal, or even domestic garbage), the *in situ* absorption of the pollutants deriving from the combustion (e.g. limestone particles absorbing SO_2), the action of a catalyst (e.g. in oil cracking), and others. In order for the bed to fulfill these functions, it is desirable that it remain homogeneous, which is exceedingly difficult to obtain. Indeed, under most

conditions, one observes large volumes of fluid, called bubbles, which contain a much smaller concentration of particles than the average, and which rise through the bed venting at its surface. In the regime commonly called "channeling," these particle-free fluid structures span the entire height of the bed. It is evident that both bubbling and channeling reduce the effectiveness of the system as they cause a large fraction of the fluid to leave the bed contacting only a limited number of particles. The transition from the state of uniform fluidization to the bubbling regime is thought to be the result of an instability which is still incompletely understood after several decades of study. The resulting uncertainty hampers both design tasks, such as scale-up, and performance, by requiring operation with conservative safety margins. Several different types of fluidized beds exist. Figure 1.1 shows a diagram of a *circulating* fluidized bed, so called because the particles are ejected from the top of the riser and then returned to the bed. The figure illustrates the wide variety of situations encountered in this system: the dense particle flow in the standpipe, the fast and dilute flow in the riser, the balance between centrifugal and gravitational forces in the cyclones, and wall effects.

It is evident that a system of this complexity is way beyond the reach of direct numerical simulation. Indeed, the mathematical models in use rely on averaged equations which, however, still suffer from several problems as will be explained in Chapters 8 and 10. Attempts to improve these equations must rely on a good understanding of the flow through assemblies of particles or, at the very least, of the flow around a particle suspended in a fluid stream, possibly spatially non-uniform and temporally varying. Furthermore, interactions with the walls are important. These considerations are a powerful motivation for the development of numerical methods for the detailed simulation of particle–fluid flow. Some methods suitable for this purpose are described in Chapters 4 and 5 of this book.

An important natural phenomenon involving fluid–particle interactions is *sediment transport* in rivers, coastal areas, and others. A significant difference with the case of fluidized beds is that, in this case, gravity tends to act orthogonally to the mean flow. This circumstance greatly affects the balance of forces on the particles, increasing the importance of lift. This component of the hydrodynamic force on bodies of a general shape is still insufficiently understood and, again, the computational methods described in Chapters 2–5 are an effective tool for its investigation.

A *bubble column* is the gas–liquid analog of a fluidized bed. The bubbles are introduced at the bottom of a liquid-filled column with the purpose of increasing the interfacial area available for a gas–liquid chemical reaction,

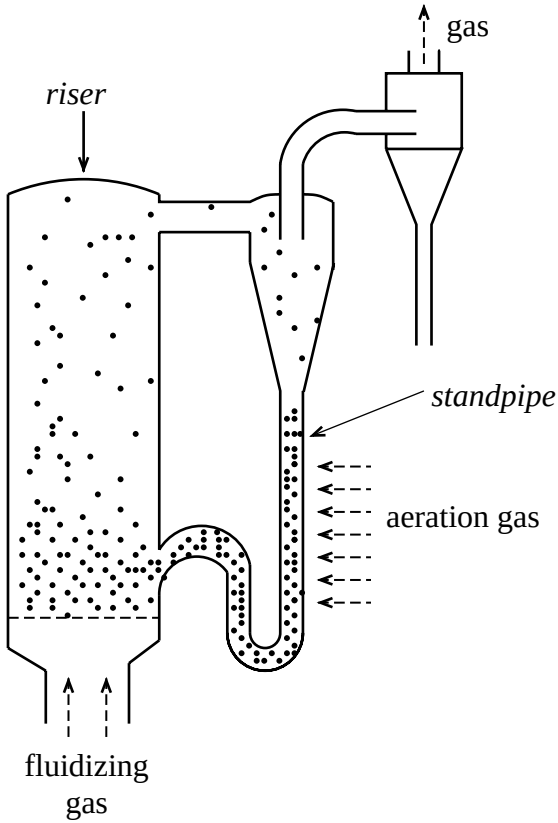

Fig. 1.1. This figure shows schematically one of several different configurations of a circulating fluidized bed loop used in engineering practice. The particles flow downward through the aerated "standpipe," and enter the bottom of a fast fluidized bed "riser." The particles are centrifugally separated from the gas in a train of "cyclones." In this diagram, the particles separated in the primary cyclone are returned to the standpipe while the fate of the particles removed from the secondary cyclone is not shown.

of aerating the liquid, or even to lift the liquid upward in lieu of a pump. Spatial inhomogeneities arise in systems of this type as well, and their effect can be magnified by the occurrence of coalescence which may produce very large gas bubbles occupying nearly the entire cross-section of the column and separated by so-called liquid "slugs." The transition from a bubbly to a slug-flow regime is a typical phenomenon of gas–liquid flows, of great practical importance but still poorly understood. Here, in addition to understanding how the bubbles arrange themselves in space, it is necessary to model the

forces which cause coalescence and the coalescence process itself. These are evidently major challenges in free-surface flows: Chapters 10 and 11 describe some computational methods capable of shedding light on such phenomena.

Another system in which coalescence plays a major role is in *clouds* and rain formation. Small water droplets fall very slowly and are easy prey to the convective motions of the atmosphere. For rain to fall, the drops need to grow to a sufficient size. Condensation is impeded by the slowness of vapor diffusion through the air to reach the drop surface. The only possible explanation of the observed short time scale for rain formation is the occurrence of coalescence. Simple random collisions caused by turbulence are very unlikely in dilute conditions. Rather, the process must rely on a subtler influence of turbulence which can be studied with the aid of an approximation in which the finite size of the droplets is (partially) disregarded. This approach to the study of turbulence–particle interaction is a powerful one described in Chapter 9. This is another example in which a critical ingredient to improve modeling is a better understanding of fluctuating hydrodynamic forces on particle assemblies which can only be gained by computational means.

Other important gas–liquid flows occur in *pipelines*. Here free gas may exist because it is originally present at the inlet, as in many oil pipelines, but it may also be due to the ex-solution of gases originally dissolved in the liquid as the pressure along the pipeline falls. Depending on the liquid and gas flow rates and on the slope of the pipeline, one may observe a whole variety of flow regimes such as bubbly, stratified, wavy, slug, annular, and others. Each one of them reacts differently to an imposed pressure gradient. For example, in a stratified flow, a given pressure drop would produce a much larger flow rate of the gas phase than of the liquid phase, unlike a bubbly or slug-flow regime. In slug flow, solid surfaces such as pumps and tube walls are often subjected to large fluctuating forces which may cause dangerous vibration and fatigue. It is therefore of great practical importance to be able to predict which flow regime would occur in a given situation, the operational limits to remain in the desired regime, and how the system would react to transients such as start-ups and shut-downs. The experimental effort devoted to this subject has been very considerable, but progress has proven to be frustratingly slow and elusive. The computational methods described in Chapters 3, 10, and 11 are promising tools for a better understanding of these problems.

Even remaining at the level of the momentum coupling between the phases, all of the examples described so far are challenging enough that a complete understanding is not yet available. When energy coupling becomes

important, such as in combustion and boiling, the difficulties increase and, with them, the prospect of progress by computational means. *Boiling* is the premier process by which electric power is generated world-wide, and is considered to be a vital means of heat removal in the computers of the future and human activities in space. Yet, this is another instance of those processes which have been very reluctant to yield their secrets in spite of nearly a century of experimental and theoretical work. Vital questions such as nucleation site density, bubble–bubble interaction, and critical heat flux are still for the most part unanswered. For space applications, understanding the role of gravity is an absolute prerequisite but microgravity experimentation is costly and fraught with difficulties. Once again, computation is a most attractive proposition. In this book, space constraints prevent us from getting very far into the treatment of nonadiabatic multiphase flow. A very brief treatment of energy coupling in the context of averaged equations is presented in Chapter 11.

1.2 A guided tour

The book can be divided into two parts, arranged in order of increasing complexity of the systems for which the methods described can be used. The first part, consisting of Chapters 2–7, describes methods suitable for the detailed solution of the Navier–Stokes equations for typical situations of interest in multiphase flow. Chapter 8 introduces the concept of averaged equations, and methods for their solution take up the second part of the book, Chapters 9 to 11.

In Chapter 2 we introduce the idea of direct numerical simulation of multiphase flows, discussing the motivation behind such simulations and what to expect from the results. We also give a brief overview of the various numerical methods used for such simulations and present in some detail elementary techniques for the solution of the Navier–Stokes equations. In Chapter 3, numerical methods for fluid–fluid simulations are discussed. The methods presented all rely on the use of a fixed Cartesian grid to solve the fluid equations, but the phase boundary is tracked in different ways, using either marker functions or connected marker particles. Computation of flows over stationary solid particles is discussed in Chapter 4. We first give an overview of methods based on the use of fixed Cartesian grids, along similar lines as the methods presented in Chapter 3, and then move on to methods based on body-fitted grids. While less versatile, these latter methods are capable of producing very accurate results for relatively high Reynolds number, thus providing essentially exact solutions that form the basis for

the modeling of forces on single particles. Simulations of more complex solid-particle flows are introduced in Chapter 5, where several versions of finite element arbitrary Lagrangian–Eulerian methods, based on unstructured tetrahedron grids that adapt to the particles as they move, are used to simulate several moving solid particles. One of the important applications of simulations of this type may be in formulating closures of the averaged quantities necessary for the modeling of multiphase flows in average terms. Chapter 6 introduces the lattice Boltzman method for multiphase flows and in Chapter 7 we discuss boundary integral methods for Stokes flows of two immiscible fluids or solid particles in a viscous fluid. While restricted to a somewhat special class of flows, boundary integral methods can reduce the computational effort significantly and yield very accurate results.

Chapters 8–11 constitute the second part of the book and deal with situations for which the direct solution of the Navier–Stokes equations would require excessive computational resources and the use of reduced descriptions becomes necessary. The basis for these descriptions is some form of averaging applied to the exact microscopic laws and, accordingly, the first chapter of this group outlines the averaging procedure and illustrates how the various reduced descriptions in the literature and in the later chapters are rooted in it. A useful approximate treatment of disperse flows – primarily particles suspended in a gas – is based on the use of point-particle models, which are considered in Chapter 9. In these models, the fluid momentum equation is augmented by point forces which represent the effect of the particles, while the particle trajectories are calculated in a Lagrangian fashion by adopting simple parameterizations of the fluid-dynamic forces. The fluid component of the model, therefore, looks very much like the ordinary Navier–Stokes equations, and it can be treated by the same methods developed for single-phase computational fluid dynamics. At present, this is the only well-developed reduced-description approach capable of incorporating the direct numerical simulation of turbulence, and efforts are currently under way to apply to it the ideas and methods of large-eddy simulation.

The point-particle model is only valid when the particle concentration is so low that particle–particle interactions can be neglected, and the particles are smaller than the smallest flow length scale, e.g. in turbulent flow, the Kolmogorv scale. Therefore, while useful, the range of applicability of the approach is rather limited. The following two chapters deal with models based on a different philosophy of broader applicability, that of *interpenetrating continua*. In the underlying conceptual picture it is supposed that the various phases are simultaneously present in each volume element in proportions which vary with time and position. Each phase is described by

a continuity, momentum, and energy equation, all of which contain terms describing the exchange of mass, momentum, and energy among the phases. Numerically, models of this type pose special challenges due to the nearly omnipresent instabilities of the equations, the constraint that the volume fractions occupied by each phase necessarily lie between 0 and 1, and many others.

In principle, the interpenetrating-continua modeling approach is very broadly applicable to a large variety of situations. A model suitable for one application, for example stratified flow in a pipeline, differs from that applicable to a different one, for example, pneumatic transport, mostly in the way in which the interphase interaction terms are specified. It turns out that, for computational purposes, most of these specific models share a very similar structure. A case in point is the vast majority of multiphase flow models adopted in commercial codes. Two broad classes of numerical methods are available. In the first one, referred to as the *segregated* approach and described in Chapter 10, the various balance equations are solved sequentially in an iterative fashion starting from an equation for the pressure. The general idea is derived from the well-known $SIMPLE$ method of single-phase computational fluid mechanics. The other class of methods, described in Chapter 11, adopts a more coupled approach to the solution of the equations and is suitable for faster transients with stronger interactions among the phases.

1.3 Governing equations and boundary conditions

In view of the prominent role played by the incompressible single-phase Navier–Stokes equations throughout this book, it is useful to summarize them here. It is assumed that the reader has a background in fluid mechanics and, therefore, no attempt at a derivation or an in-depth discussion will be made. Our main purpose is to set down the notation used in later chapters and to remind the reader of some fundamental dimensionless quantities which will be frequently encountered.

If $\rho(\mathbf{x}, t)$ and $\mathbf{u}(\mathbf{x}, t)$ denote the fluid density and velocity fields at position $\mathbf{x}$ and time t, the equation of continuity is

$$\frac{\partial \rho}{\partial t} + \boldsymbol{\nabla} \cdot (\rho \mathbf{u}) = 0. \tag{1.1}$$

For incompressible flows this equation reduces to

$$\boldsymbol{\nabla} \cdot \mathbf{u} = 0. \tag{1.2}$$

This latter equation embodies the fact that each fluid particle conserves its volume as it moves in the flow.

In conservation form, the momentum equation is

$$\frac{\partial}{\partial t}(\rho \mathbf{u}) + \boldsymbol{\nabla} \cdot (\rho \mathbf{u}\mathbf{u}) = \boldsymbol{\nabla} \cdot \boldsymbol{\sigma} + \rho \mathbf{f}, \tag{1.3}$$

in which $\mathbf{f}$ is an external force per unit volume acting on the fluid. Very often, the force $\mathbf{f}$ will be the acceleration of gravity $\mathbf{g}$. However, as in Chapter 9, one may think of very small suspended particles as exerting point forces which can also be described by the field $\mathbf{f}$. The stress tensor $\boldsymbol{\sigma}$ may be decomposed into a pressure p and viscous part $\boldsymbol{\tau}$:

$$\boldsymbol{\sigma} = -p\mathbf{I} + \boldsymbol{\tau}, \tag{1.4}$$

in which $\mathbf{I}$ is the identity two-tensor. In most of the applications that follow, we will be dealing with Newtonian fluids, for which the viscous part of the stress tensor is given by

$$\boldsymbol{\tau} = 2\mu \mathbf{e}, \qquad \mathbf{e} = \frac{1}{2}\left(\boldsymbol{\nabla}\mathbf{u} + \boldsymbol{\nabla}\mathbf{u}^{\mathrm{T}}\right), \tag{1.5}$$

in which μ is the coefficient of (dynamic) viscosity, $\mathbf{e}$ the rate-of-strain tensor, and the superscript T denotes the transpose; in component form:

$$e_{ij} = \frac{1}{2}\left(\frac{\partial u_i}{\partial x_j} + \frac{\partial u_j}{\partial x_i}\right), \tag{1.6}$$

in which $\mathbf{x} = (x_1, x_2, x_3)$. With (1.5), (1.3) takes the familiar form of the Navier–Stokes momentum equation for a Newtonian, constant-properties fluid:

$$\frac{\partial \mathbf{u}}{\partial t} + \boldsymbol{\nabla} \cdot (\mathbf{u}\mathbf{u}) = -\frac{1}{\rho}\boldsymbol{\nabla} p + \nu \boldsymbol{\nabla}^2 \mathbf{u} + \mathbf{f}, \tag{1.7}$$

in which $\nu = \mu/\rho$ is the kinematic viscosity. Because of (1.2), this equation may be written in non-conservation form as

$$\frac{\partial \mathbf{u}}{\partial t} + (\mathbf{u} \cdot \boldsymbol{\nabla})\,\mathbf{u} = -\frac{1}{\rho}\boldsymbol{\nabla} p + \nu \nabla^2 \mathbf{u} + \mathbf{f}, \tag{1.8}$$

where the notation implies that the i-th component of the second term is given by

$$\left[(\mathbf{u} \cdot \boldsymbol{\nabla})\,\mathbf{u}\right]_i = \sum_{j=1}^{3} u_j \frac{\partial u_i}{\partial x_j}. \tag{1.9}$$

When the force field $\mathbf{f}$ admits a potential $\mathcal{U}$, $\mathbf{f} = -\boldsymbol{\nabla}\mathcal{U}$, one may introduce

the *reduced* or *modified pressure*, i.e. the pressure in excess of the hydrostatic contribution,

$$p^{\mathrm{r}} = p + \rho\mathcal{U} \tag{1.10}$$

in terms of which (1.8) becomes

$$\frac{\partial \mathbf{u}}{\partial t} + (\mathbf{u}\cdot\boldsymbol{\nabla})\,\mathbf{u} = -\frac{1}{\rho}\boldsymbol{\nabla}p^{\mathrm{r}} + \nu\nabla^2\mathbf{u}. \tag{1.11}$$

In particular, for the gravitational force, $\mathcal{U} = -\rho\mathbf{g}\cdot\mathbf{x}$.

We have already noted at the beginning of this chapter that multiphase flows are often characterized by the presence of interfaces. When there is a mass flux $\dot{m}$ across (part of) the boundary S separating two phases 1 and 2 as, for example, in the presence of phase change at a liquid–vapor interface, conservation of mass requires that

$$\dot{m} \equiv \rho_2\,(\mathbf{u}_2 - \mathbf{w})\cdot\mathbf{n} = \rho_1\,(\mathbf{u}_1 - \mathbf{w})\cdot\mathbf{n} \tag{1.12}$$

where $\mathbf{n}$ is the unit normal and $\mathbf{w}\cdot\mathbf{n}$ the normal velocity of the interface itself. An expression for this quantity is readily found if the interface is represented as

$$S(\mathbf{x}, t) = 0. \tag{1.13}$$

Indeed, at time $t + dt$, we will have $S(\mathbf{x} + \mathbf{w}dt, t + dt) = 0$ from which, after a Taylor series expansion,

$$\frac{\partial S}{\partial t} + \mathbf{w}\cdot\boldsymbol{\nabla}S = 0 \qquad \text{on} \qquad S = 0. \tag{1.14}$$

But the unit normal, directed from the region where $S < 0$ to that where $S > 0$, is given by

$$\mathbf{n} = \frac{\boldsymbol{\nabla}S}{|\boldsymbol{\nabla}S|}, \tag{1.15}$$

so that

$$\mathbf{n}\cdot\mathbf{w} = -\frac{1}{|\boldsymbol{\nabla}S|}\frac{\partial S}{\partial t}. \tag{1.16}$$

If $S = 0$ denotes an impermeable surface, as in the case of a solid wall, $\dot{m} = 0$ so that $\mathbf{n}\cdot\mathbf{u} = \mathbf{n}\cdot\mathbf{w}$. In this case, by (1.12), (1.16) becomes the so-called *kinematic boundary condition*:

$$\frac{\partial S}{\partial t} + \mathbf{u}\cdot\boldsymbol{\nabla}S = 0 \qquad \text{on} \qquad S = 0. \tag{1.17}$$

At solid surfaces, for viscous flow, one usually imposes the *no-slip* condition,

which requires the tangential velocity of the fluid to match that of the boundary:

$$\mathbf{n} \times (\mathbf{u} - \mathbf{w}) = 0 \qquad \text{on} \qquad S = 0. \tag{1.18}$$

(It is well known that there are situations, such as contact line motion, where this relation does not reflect the correct physics. Several more or less *ad hoc* models to treat these cases exist, but a "standard" one has yet to emerge.) Upon combining (1.14) and (1.18) one simply finds, for an impermeable surface,

$$\mathbf{u} = \mathbf{w} \qquad \text{on} \qquad S = 0. \tag{1.19}$$

The tangential velocity of a fluid interface can only be unambiguosly defined when the interface points carry some attribute other than their geometric location in space, such as the concentration of a surfactant[1]. For a purely geometric interface, the tangential velocity is meaningless as a mapping of the interface on itself cannot have physical consequences. For example, in the case of an expanding sphere such as a bubble, a rotation around the fixed center cannot have quantitative effects. In the case of two fluids separated by a purely geometric interface, the velocity field of each fluid must individually satisfy (1.17) but, rather than (1.18), the proper condition is one of continuity of the tangential velocity:

$$\mathbf{n} \times (\mathbf{u}_1 - \mathbf{u}_2) = 0. \tag{1.20}$$

It is interesting to note that, while both (1.18) and (1.20) are essentially phenomenological relations, in the case of inviscid fluids with a constant surface tension (1.20) is actually a consequence of the conservation of tangential momentum provided $\dot{m} \neq 0$. When $\dot{m} = 0$, the combination of (1.17) for each fluid and (1.20) renders the entire velocity continuous across the interface:

$$\mathbf{u}_1 = \mathbf{u}_2 \qquad \text{on} \qquad S = 0. \tag{1.21}$$

When the interface separates a liquid from a gas or a vapor, the dynamical effects of the latter can often be modeled in terms of pressure alone, neglecting viscosity. In this case, only the normal condition (1.17) applies, but not the tangential condition (1.20).

For solid boundaries with a prescribed velocity, the condition (1.19), possibly augmented by suitable conditions at infinity and at the initial instant, is sufficient to find a well-defined solution to the Navier–Stokes equations (1.2)

[1] In spite of its simplicity, the interface model described here is often adequate for many applications. Much more sophisticated models exist as described, for example, in Edwards *et al.* (1991).

and (1.7) or (1.8). For a free surface, a further condition is required to determine the motion of the surface itself. This condition arises from a momentum balance across the interface which stipulates that the jump in the surface tractions $\mathbf{t} = \boldsymbol{\sigma} \cdot \mathbf{n}$, combined with the momentum fluxes, be balanced by the action of surface tension:

$$(\boldsymbol{\sigma}_2 - \boldsymbol{\sigma}_1) \cdot \mathbf{n} - \dot{m} (\mathbf{u}_2 - \mathbf{u}_1) = -\boldsymbol{\nabla} \cdot [(\boldsymbol{I} - \mathbf{nn}) \gamma] = -(\boldsymbol{I} - \mathbf{nn}) \cdot \boldsymbol{\nabla}\gamma + \gamma\kappa\mathbf{n}, \tag{1.22}$$

where γ is the surface tension coefficient and

$$\kappa = \boldsymbol{\nabla} \cdot \mathbf{n}, \tag{1.23}$$

the local mean curvature of the surface. It will be recognized that $\boldsymbol{I} - \mathbf{nn}$ is the projector on the plane tangent to the interface. The signs in Eq. (1.22) are correct provided S is defined so that $S > 0$ in fluid 2 and $S < 0$ in fluid 1. In practice, it is more convenient to decompose this condition into its normal and tangential parts. The former is

$$-p_2 + p_1 + \mathbf{n} \cdot (\boldsymbol{\tau}_2 - \boldsymbol{\tau}_1) \cdot \mathbf{n} - \dot{m} (\mathbf{u}_2 - \mathbf{u}_1) \cdot \mathbf{n} = \gamma\kappa \tag{1.24}$$

while the tangential component is, by (1.18),

$$\mathbf{n} \times (\boldsymbol{\tau}_2 - \boldsymbol{\tau}_1) \cdot \mathbf{n} = -(\boldsymbol{I} - \mathbf{nn}) \cdot \boldsymbol{\nabla}\gamma. \tag{1.25}$$

If, in place of p, the reduced pressure p^{r} defined in (1.10) is used, the right-hand sides of (1.22) and (1.24) acquire an additional contribution necessary to cancel the difference between the potentials $\mathcal{U}$ in the two fluids; for example, (1.24) becomes

$$-p_2^{\mathrm{r}} + p_1^{\mathrm{r}} + \mathbf{n} \cdot (\boldsymbol{\tau}_2 - \boldsymbol{\tau}_1) \cdot \mathbf{n} = \gamma\kappa + \rho_1\mathcal{U}_1 - \rho_2\mathcal{U}_2. \tag{1.26}$$

Let us now consider a rigid body of mass m_{b}, inertia tensor $\mathbf{J}_{\mathrm{b}}$, volume $\mathcal{V}_{\mathrm{b}}$ and surface S_{b} immersed in the fluid. According to the laws of dynamics, the motion of such a body is governed by an equation specifying the rate of change of the linear momentum

$$\frac{d}{dt}(m_{\mathrm{b}}\mathbf{v}) = \mathbf{F}^{\mathrm{h}} + \mathbf{F}^{\mathrm{e}} + m_{\mathrm{b}}\mathbf{g}, \tag{1.27}$$

and of the angular momentum

$$\frac{d}{dt}(\mathbf{J}_{\mathrm{b}} \cdot \boldsymbol{\Omega}) = \mathbf{L}^{\mathrm{h}} + \mathbf{L}^{\mathrm{e}}. \tag{1.28}$$

Here $\mathbf{v}$ is the velocity of the body center of mass, $\boldsymbol{\Omega}$ the angular velocity about the center of mass, and $\mathbf{F}$ and $\mathbf{L}$ denote forces and couples,

respectively; the superscripts "h" and "e" distinguish between forces and couples of hydrodynamic and other, external, origin. The former are given by

$$\mathbf{F}^{\mathrm{h}} = \int_{S_{\mathrm{b}}} \boldsymbol{\sigma} \cdot \mathbf{n}\, dS_{\mathrm{b}}, \qquad \mathbf{L}^{\mathrm{h}} = \int_{S_{\mathrm{b}}} \mathbf{x} \times [\boldsymbol{\sigma} \cdot \mathbf{n}]\, dS_{\mathrm{b}}, \tag{1.29}$$

where $\mathbf{x}$ is measured from the center of mass and the unit normal $\mathbf{n}$ is directed outward from the body. When the fluid stress in $\mathbf{F}^{\mathrm{h}}$ is expressed in terms of the ordinary pressure p, the buoyancy force arises as part of the hydrodynamic force. Sometimes it may be more useful to express the fluid stress in terms of the reduced pressure p^{r} defined in (1.10). In the case of gravity, $\mathcal{U} = -\rho \mathbf{g} \cdot \mathbf{x}$ and (1.27) takes the form

$$\frac{d}{dt}\,(m_{\mathrm{b}}\mathbf{v}) = \mathbf{F}^{\mathrm{h}}_{\mathrm{r}} + \mathbf{F}^{\mathrm{e}} + (m_{\mathrm{b}} - \rho \mathcal{V}_{\mathrm{b}})\,\mathbf{g}. \tag{1.30}$$

The position $\mathbf{X}$ of the center of mass and the orientation of the body (for example, the three Euler angles), $\boldsymbol{\Theta}$, depend on time according to the kinematic relations

$$\frac{d\mathbf{X}}{dt} = \mathbf{v}, \qquad \frac{d\boldsymbol{\Theta}}{dt} = \boldsymbol{\Omega}, \tag{1.31}$$

respectively.

1.4 Some dimensionless groups

The use of dimensional analysis and dimensionless groups is a well-established practice in ordinary fluid dynamics and it is no less useful in multiphase flow. Each problem will have one or more characteristic length scales such as particle size, duct diameter, and others. The spatial scale of each problem can therefore be represented by a characteristic length L and, possibly, dimensionless ratios of the other scales to L. A similar role may be played by an intrinsic time scale τ due, for example, to an imposed time dependence of the flow or a force oscillating with a prescribed frequency, and by a velocity scale U. We introduce dimensionless variables $\mathbf{x}_*$, t_*, and $\mathbf{u}_*$ by writing

$$\mathbf{x} = L\mathbf{x}_*, \qquad t = \tau t_*, \qquad \mathbf{u} = U\mathbf{u}_*. \tag{1.32}$$

Furthermore, we let

$$\boldsymbol{\nabla} p = \frac{\Delta P}{L} \boldsymbol{\nabla}_* p_*, \qquad \mathbf{f} = f\mathbf{f}_* \tag{1.33}$$

where $\boldsymbol{\nabla}_*$ denotes the gradient operator with respect to the dimensionless coordinate $\mathbf{x}_*$, ΔP is an appropriate pressure-difference scale, and f

a representative value of **f**. Then the continuity equation remains formally unaltered,

$$\boldsymbol{\nabla}_* \cdot \mathbf{u}_* = 0, \tag{1.34}$$

while the momentum equation (1.8) becomes

$$\frac{1}{Sl}\frac{\partial \mathbf{u}_*}{\partial t_*} + (\mathbf{u}_* \cdot \boldsymbol{\nabla}_*)\,\mathbf{u}_* = -\frac{\Delta p}{\rho U^2}\boldsymbol{\nabla}_* p_* + \frac{1}{Re}\nabla_*^2 \mathbf{u}_* + \frac{fL}{U^2}\mathbf{f}_*. \tag{1.35}$$

Here we have introduced the *Strouhal number Sl*, defined by

$$Sl = \frac{U\tau}{L}, \tag{1.36}$$

which expresses the ratio of the intrinsic time scale τ to the convective time scale L/U. When no external or imposed time scale is present, $\tau = L/U$ and $Sl = 1$. The *Reynolds number Re* is defined by

$$Re = \frac{\rho LU}{\mu} = \frac{LU}{\nu}, \tag{1.37}$$

and, in addition to its usual meaning of the ratio of inertial to viscous forces, can be interpreted as the ratio of the viscous diffusion time L^2/ν to the convective time scale L/U. When the force **f** is gravity, $f = g = |\mathbf{g}|$ and the group

$$Fr = \frac{U^2}{gL} \tag{1.38}$$

is known as the *Froude number*.

The appropriate pressure-difference scale depends on the situation. When fluid inertia is important, pressure differences scale proportionally to ρU^2 so that we may take $\Delta P = \rho U^2$ to find

$$\frac{1}{Sl}\frac{\partial \mathbf{u}_*}{\partial t_*} + (\mathbf{u}_* \cdot \boldsymbol{\nabla}_*)\,\mathbf{u}_* = -\boldsymbol{\nabla}_* p_* + \frac{1}{Re}\nabla_*^2 \mathbf{u}_* + \frac{fL}{U^2}\mathbf{f}_*. \tag{1.39}$$

Frequently $Sl = 1$ and this equation becomes

$$\frac{\partial \mathbf{u}_*}{\partial t_*} + (\mathbf{u}_* \cdot \boldsymbol{\nabla}_*)\,\mathbf{u}_* = -\boldsymbol{\nabla}_* p_* + \frac{1}{Re}\nabla_*^2 \mathbf{u}_* + \frac{fL}{U^2}\mathbf{f}_*. \tag{1.40}$$

On the other hand, when the flow is dominated by viscosity, the proper pressure scale is $\Delta P = \mu U/L$ and the equation becomes

$$\frac{1}{Sl}\frac{\partial \mathbf{u}_*}{\partial t_*} + (\mathbf{u}_* \cdot \boldsymbol{\nabla}_*)\,\mathbf{u}_* = -\frac{1}{Re}\boldsymbol{\nabla}_* p_* + \frac{1}{Re}\nabla_*^2 \mathbf{u}_* + \frac{fL}{U^2}\mathbf{f}_*. \tag{1.41}$$

A special situation arises when $Re \ll 1$ and $Re/Sl = (L^2/\nu)/\tau \ll 1$ as,

then, the left-hand side of this equation is negligible; in dimensional form, what remains is

$$-\boldsymbol{\nabla} p + \mu \nabla^2 \mathbf{u} + \rho \mathbf{f} = 0, \tag{1.42}$$

which, together with (1.34), are known as the *Stokes equations*.

Additional dimensionless groups arise from the boundary conditions. In the case of inertia-dominated pressure scaling, the normal stress condition (1.24) leads to

$$-p_{*2} + p_{*1} + \frac{1}{Re}\mathbf{n} \cdot (\boldsymbol{\tau}_{*2} - \boldsymbol{\tau}_{*1}) \cdot \mathbf{n} = \frac{1}{We}\kappa_* \tag{1.43}$$

where $\kappa_* = L\kappa$ and the *Weber number*, expressing the ratio of inertial and surface-tension-induced pressures, is defined by

$$We = \frac{\rho L U^2}{\gamma}. \tag{1.44}$$

In some cases, the characteristic velocity is governed by buoyancy, which leads to the estimate $U \sim \sqrt{(|\rho - \rho'|/\rho)gL}$. A typical case is the rise of large gas bubbles (density ρ') in a free liquid or in a liquid-filled tube. In these cases, equation (1.44) becomes

$$Eo = Bo = \frac{|\rho - \rho'| g L^2}{\gamma}, \tag{1.45}$$

a combination known as the *Eötvös number* or *Bond number*. When $\rho' \ll \rho$, Eo is simply written as

$$Eo = \frac{\rho g L^2}{\gamma}. \tag{1.46}$$

The *Morton number*, defined by

$$Mo = \frac{g\mu^4}{\rho\gamma^3}, \tag{1.47}$$

is often useful as, for fixed g, it only depends on the liquid properties. If the Reynolds number is expressed in terms of the characteristic velocity $\sqrt{gL}$, one immediately verifies that $Mo = (Eo^3/Re^4)$. The Reynolds number constructed with the velocity $\sqrt{(|\rho - \rho'|/\rho)gL}$ is the *Galilei number*

$$Ga = \frac{\sqrt{g\rho|\rho - \rho'|L^3}}{\mu}. \tag{1.48}$$

In the opposite case of viscosity-dominated pressure scaling, the normal-stress condition (1.24) becomes

$$-p_{*2} + p_{*1} + \mathbf{n} \cdot (\boldsymbol{\tau}_{*2} - \boldsymbol{\tau}_{*1}) \cdot \mathbf{n} = \frac{1}{Ca}\kappa_* \tag{1.49}$$

where the *capillary number*, expressing the ratio of viscous to capillary stresses, is defined by

$$Ca = \frac{\mu U}{\gamma}. \tag{1.50}$$

For small-scale phenomena dominated by surface tension and viscosity, the characteristic time due to the flow, L/U, is of the order of $\sqrt{\rho L^3/\gamma}$, while the intrinsic time scale is the diffusion time L^2/ν. In this case the inverse of the Strouhal number (1.36) is known as the *Ohnesorge number*

$$Oh = \frac{\mu}{\sqrt{\rho \gamma L}}. \tag{1.51}$$

An important dimensionless parameter governing the dynamics of a particle in a flow is the *Stokes number* defined as the ratio of the characteristic time of the particle response to the flow to that of the flow itself:

$$St = \frac{\tau_\mathrm{b}}{\tau}. \tag{1.52}$$

This ratio can be estimated as follows. Let U_r denote the characteristic particle–fluid relative velocity and A its projected area on a plane normal to the relative velocity. When inertia is important, the order of magnitude of the hydrodynamic force $|\mathbf{F}^\mathrm{h}|$ may be estimated in terms of a *drag coefficient* C_d defined by

$$C_\mathrm{d} = \frac{F^\mathrm{h}}{\frac{1}{2}\rho A U_\mathrm{r}^2}, \tag{1.53}$$

In problems where the scale of the relative velocity is determined by a balance between the hydrodynamic and gravity forces, U_r may be estimated as

$$U_\mathrm{r} \sim \sqrt{\frac{1}{C_\mathrm{d}} \left| \frac{\rho_\mathrm{b}}{\rho} - 1 \right| L\, g} \tag{1.54}$$

where ρ_b is the density of the body and $L = \mathcal{V}_\mathrm{b}/A$ is a characteristic body length defined in terms of the body volume $\mathcal{V}_\mathrm{b}$. The characteristic relaxation time of the body velocity in the flow, τ_b, may be determined by balancing the left-hand side of the body momentum equation, $\rho_\mathrm{b}\mathcal{V}_\mathrm{b}U_\mathrm{r}/\tau_\mathrm{b}$, with the hydrodynamic force to find

$$\tau_\mathrm{b} \sim \frac{L}{C_\mathrm{d} U_\mathrm{r}} \frac{\rho_\mathrm{b}}{\rho} \sim \frac{\rho_\mathrm{b}}{\rho} \sqrt{\frac{L}{C_\mathrm{d}\, |\rho_\mathrm{b}/\rho - 1|\, g}}. \tag{1.55}$$

When the Reynolds number of the relative motion, $Re_\mathrm{b} = LU_\mathrm{r}/\nu$, is small,

$C_{\rm d} \simeq 1/Re_{\rm b}$ and we have

$$U_{\rm r} \sim \left| \frac{\rho_{\rm b}}{\rho} - 1 \right| \frac{L^2 g}{\nu}, \qquad \text{from which} \qquad \tau_{\rm b} \sim \frac{\rho_{\rm b}}{\rho} \frac{L^2}{\nu} \tag{1.56}$$

so that

$$St \sim \frac{\rho_{\rm b}}{\rho} \frac{L^2}{\nu\tau}. \tag{1.57}$$

In particular, for a sphere of radius a, $\tau_{\rm b} = 2\rho_{\rm b} a^2/(9\rho\nu)$ and one finds

$$St = \frac{2\rho_{\rm b} a^2}{9\mu\tau}. \tag{1.58}$$